Tolerancing of diffraction-limited Kirkpatrick–Baez synchrotron beamline optics for extreme-ultraviolet metrology

Patrick P. Naulleau, Kenneth A. Goldberg, Phillip J. Batson, Seongtae Jeong, and James H. Underwood

The recent interest in extreme-ultraviolet (EUV) lithography has led to the development of an array of at-wavelength metrologies implemented on synchrotron beamlines. These beamlines commonly use Kirkpatrick–Baez (K–B) systems consisting of two perpendicular, elliptically bent mirrors in series. To achieve high-efficiency focusing into a small spot, unprecedented fabrication and assembly tolerance is required of these systems. Here we present a detailed error-budget analysis and develop a set of specifications for diffraction-limited performance for the K–B optic operating on the EUV interferometry beamline at Lawrence Berkeley National Laboratory's Advanced Light Source. The specifications are based on CODE V modeling tools developed explicitly for these optical systems. Although developed for one particular system, the alignment sensitivities presented here are relevant to K–B system designs in general. © 2001 Optical Society of America

OCIS codes: 340.6720, 220.2740, 220.4830, 220.1010, 220.1140.

1. Introduction

The recent interest in extreme-ultraviolet (EUV) lithography[1] has led to the development of a variety of novel metrologies. Because EUV optical systems use resonant-stack, reflective multilayer-coated optics,[2] metrology performed at the operational wavelength is essential to the development process.[3] Some of the recently developed EUV metrologies include wave-front measuring interferometry,[4–7] flare measurement techniques,[8,9] reflection-multilayer-mask defect inspection,[10] and high-accuracy reflectometry.[11] The majority of these at-wavelength metrologies utilize synchrotron radiation because of its high brightness and stability characteristics.

A key component of many beamline designs is a Kirkpatrick–Baez (K–B)[12] mirror system used for two-dimensional focusing. This system comprises two orthogonal glancing-incidence elliptical mirrors designed for point-to-point imaging. Each mirror is elliptically profiled in only one dimension (i.e., cylindrical ellipses), and the two-dimensional focusing property of the system is provided by the orthogonal combination of the two mirrors. The elliptical shape is most conveniently achieved through bending techniques in which thin, nominally flat, width-profiled mirrors are bent and held in the desired shape.[13–16] The width profiles are designed such that the desired elliptical shapes are obtained when the proper bend forces are applied to the ends of each mirror.

Nearly diffraction-limited performance from the K–B system is essential to several of the EUV metrologies listed above. This is especially true for the EUV phase-shifting point-diffraction interferometer[6–8] where a spatial-filtering pinhole is placed at the focus of the K–B system to illuminate the optic under test with a highly coherent and ideally spherical probe beam. The necessarily small size of the spatial-filter pinhole requires a high-efficiency, fine-spatial-resolution beamline for the interferometer to achieve adequate throughput. For example, to test a 5×-reduction, 0.3-numerical aperture optic operating at a wavelength of 13.4 nm, a spatial-filtering pinhole diameter of approximately 100 nm at the focus of the K–B system would be required. Another at-wavelength metrology for which diffraction-limited performance is of paramount concern is EUV mask defect inspection in which the goal is to detect

The authors are with the Center for X-Ray Optics, Lawrence Berkeley National Laboratory, Berkeley, California 94720. P. Naulleau's e-mail address is pnaulleau@lbl.gov.

Received 20 February 2001; revised manuscript received 28 April 2001.
0003-6935/01/223703-07$15.00/0
© 2001 Optical Society of America

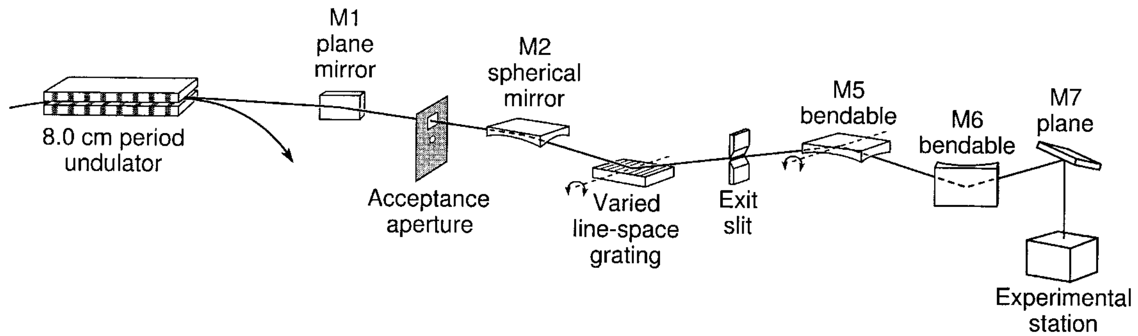

Fig. 1. Schematic of the EUV interferometry beamline at the Advanced Light Source synchrotron radiation facility at Lawrence Berkeley National Laboratory. This beamline produces a demagnified image of the undulator source at the focal plane of the K–B, corresponding to the entrance plane of the experimental station.

sub-50-nm defects, and the defect sensitivity is directly proportional to the probe beam size.[10]

In practice, achieving diffraction-limited performance from a K–B system operating at EUV wavelengths has proven to be quite challenging. In our experience, the difficulties stem primarily from a lack of understanding of the fabrication and assembly tolerance requirements as well as insufficient degrees of freedom for *in situ* alignment of the system.

Here we present a detailed error-budget analysis for K–B systems and develop a set of specifications for diffraction-limited performance. The specifications are based on CODE V[17] modeling tools developed explicitly for these grazing-incidence optical systems. We also describe aberration signatures as observed in the K–B focal plane that are useful for the facilitation of *in situ* alignment. Although the motivation and specific examples described here are based on EUV applications, the methods and results presented are broadly applicable to K–B systems operating in any wavelength range.

2. Extreme-Ultraviolet Interferometry Beamline

The beamline and K–B used as the basis of the analysis presented here are part of the EUV interferometry[6–8] beamline at the Advanced Light Source synchrotron radiation facility at Lawrence Berkeley National Laboratory. This undulator beamline[18] (Fig. 1) produces a demagnified image of the source at the K–B focal plane, which corresponds to the entrance plane of the experimental station. In the horizontal direction, the K–B system directly demagnifies the source by a factor or 60, whereas in the vertical direction the K–B system reimages an intermediate vertical image plane located at the exit slit of the beamline monochromator (Fig. 1). This intermediate image is created by the combination of the M2 mirror and the varied line-space monochromator grating in Fig. 1. The vertical demagnification of the K–B is 7.2, providing an overall beamline vertical demagnification of 60, matching the horizontal demagnification. With a rectangular entrance numerical aperture of 8×10^{-5} and a demagnification of 60, the beamline has a diffraction-limited peak-to-null resolution of approximately 1.4 μm in the K–B focal plane, at a wavelength of 13.4 nm.

A computer model of the K–B system is shown in Fig. 2. The vertically focusing mirror (M5) has an object distance of 5564.71 mm, an image distance of 775.28 mm, and a central-ray angle of incidence of 84.5° off normal. The horizontally focusing mirror (M6) has an object distance of 24393.44 mm, an image distance of 406.56 mm, and a central-ray angle of incidence of 87° off normal. The center-to-center mirror separation is 361.95 mm. Both mirrors are profiled in width such that they ideally bend into elliptical shapes having foci matching the image and object distances when the appropriate bend moments are applied. For each mirror, the total mirror length between the bend actuators is 200 mm, and the mirror width is nominally 30 mm. The active (illuminated) areas of the mirrors, as determined by the 80-μrad beamline input half-angle, are 3.85 mm × 77.65 mm for M5 and 4.27 mm × 74.57 mm for M6.

The fabricated K–B system has a total of eight independent alignment actuators: two bend actuators on each mirror, tilt (angle of incidence) control on

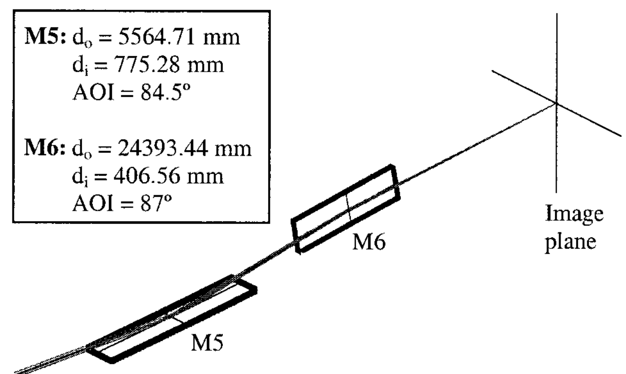

Fig. 2. Computer model of the EUV interferometry beamline K–B system. The vertically focusing mirror (M5) has an object distance d_o of 5564.71 mm, an image distance d_i of 775.28 mm, and an angle of incidence (AOI) of 84.5° from normal. The horizontally focusing mirror (M6) has an object distance of 24393.44 mm, an image distance of 406.56 mm, and an AOI of 87° from normal.

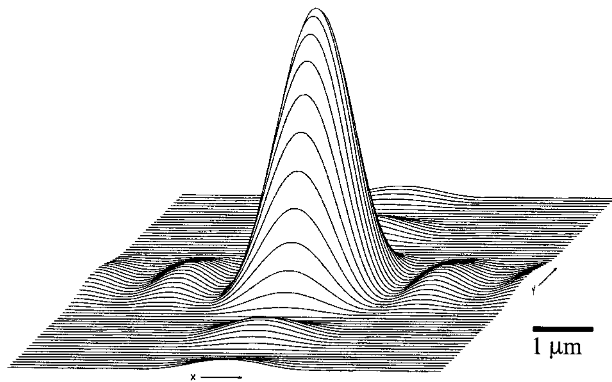

Fig. 3. CODE V calculated point-spread function for the beamline in Fig. 1 with K–B from Fig. 2. The sinc function like behavior comes from the rectangular beamline aperture.

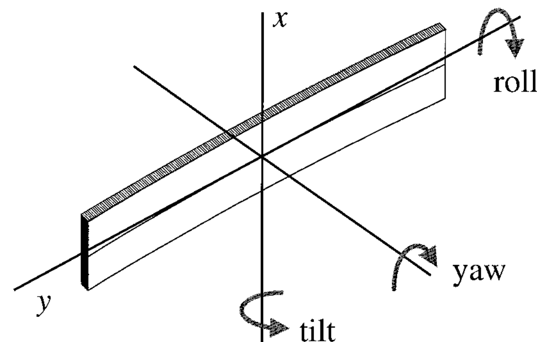

Fig. 4. Mirror coordinate axes definition.

each mirror, and twist control on one end of each mirror. The bend moments used to shape the mirrors are applied by separate actuators close to the ends of the mirrors. Tilt adjustments are made about the center of the mirror and are used to attain the correct central-ray angle of incidence. The twist control is used to correct nonparallelism between the two ends of the mirror in the cross-bend direction (the direction in which the mirror has no optical power).

In addition to the mirror-based alignment actuators described above, the K–B system also has global positioning actuators allowing it to be positioned in 6 degrees of freedom relative to the rest of the beamline.

3. CODE V Tolerancing

Although common in synchrotron optics, the K–B and other grazing-incidence systems are relatively rare among conventional optical systems and are not well supported by commercially available optical design packages. The modeling of synchrotron optics is typically done by a public domain ray-tracing package called SHADOW.[19] SHADOW, however, lacks many of the powerful features common to commercial optical design packages such as CODE V.[17] For example, SHADOW does not readily provide many of the CODE V features that facilitate the efficient tolerancing of optical systems, including direct support of wave-front and point-spread function calculation, modulation transfer function support, partially coherent imaging simulation, system visualization, and a well-developed user interface.

To support the detailed assembly and fabrication tolerancing of interest here, we extended the capabilities of CODE V by way of customized user-defined surfaces and macros[20] to model bendable, profiled, grazing-incidence optical systems. The CODE V implementation uses bent-beam theory[14,16] to model the bendable mirrors.

Figure 3 shows the CODE V calculated point-spread function for the beamline described above, operating at a wavelength of 13.4 nm. The sinc-function-like behavior comes from the rectangular beamline entrance aperture (the acceptance aperture in Fig. 1). The CODE V modeling is based on monochromatic input in which the dispersion characteristics of the monochromator grating were ignored. For the purpose of the model, the optical power provided by the varied line-space grating is incorporated into the M2 mirror. The simplified monochromatic model is equivalent to the operation of the beamline in the high-spectral-resolution regime, where the monochromator exit slit is set to be smaller than the object-side diffraction-limited vertical resolution of the K–B ($7.2 \times 1.4\ \mu m = 10\ \mu m$). Under this condition, the beamline spectral resolution ($\lambda/\Delta\lambda$) is greater than or equal to approximately 1000.

The subsequent tolerancing of the K–B is based on one determining the magnitude of each isolated error leading to a doubling of the diameter of the disk containing 53% of the point-spread function energy. In the ideal system this disk diameter is approximately equal to the 1.4-μm peak-to-null resolution quoted above. Although somewhat arbitrary, this criterion provides a computationally convenient and physically meaningful benchmark. During the tolerancing, the image-plane position is kept as a free parameter that is optimized for each error configuration. This means that a simple longitudinal focus shift is not considered as an error.

We begin by considering the system tolerance to rotation errors. The coordinate axes for each mirror are defined with x along the mirror width (lateral) and y along the mirror length (longitudinal) in the direction of the beam propagation. The various rotations are defined through the central point of the mirrors as follows: tilt is rotation about the x axis, roll is rotation about the y axis, and yaw is rotation in the plane of the mirror (Fig. 4). Table 1 shows the rotation error tolerances for M5 and M6.

K–B systems are extremely sensitive to tilt errors and relatively insensitive to yaw errors. Tilt sensitivity is high because the definition of the ideal ellipse and its foci changes rapidly as a function of the tilt angle; however, tilt errors can be largely compensated through mirror refocusing (rebending). Using compensation based on individual bend moment control on each end of the mirror, we can compensate, in principle, tilt errors as large as several degrees. In practice, however, there are limits based on the ge-

Table 1. Rotation Error Tolerances for M5 and M6[a]

Rotation	M5 (deg)	M6 (deg)
Tilt	±0.0046	±0.0054
Roll	±0.025	±0.046
Yaw	±0.44	±0.86

[a]Rotations are made about the centers of the mirrors. The axes are defined as shown in Fig. 4. Tolerances are defined as those errors that cause a doubling in the width of the point-spread function.

Table 3. Roll Error Tolerances for M5 and M6 with and without Twist and Bend Compensation[a]

Roll	M5 (deg)	M6 (deg)
Uncompensated	±0.025	±0.046
Compensated	±0.028	±0.52

[a]The uncompensated values come from Table 1. For a roll error on M5, the required compensations are twist and focus on M6. For M6 roll error, the required compensations are twist and focus on M6 or twist and focus on M5.

ometry of the system, the reflectivity of the grazing-incidence mirrors as a function of angle, and the large compensation-induced focal shifts. For the K–B system under consideration here, these practical limits constrain us to compensating tilt errors no larger than approximately 0.1°. It is therefore important to retain tilt control even if the system is equipped with bend control.

Next we consider the tolerance to twist error. Twist error arises from nonparallelism between the two ends of the mirror in the cross-bend direction, as shown in Fig. 5. Twist, which can be viewed as a roll error that varies along the length of the mirror and can be defined mathematically as sag $= Txy$, where sag is the mirror height error, T is the twist error coefficient, and x and y are the coordinates in the plane of the mirror, defined above. Table 2 shows the twist error tolerance both in terms of the twist coefficient and the peak-to-valley (PV) deflection this represents on one end of the mirror when the opposite end is assumed fixed. In our case, in which the two mirror supports are separated by 200 mm and the mirror width is 30 mm, the PV twist error will be T(200 mm)(30 mm). In the case of M5, the two ends of the mirror, which are 200 mm apart, must be parallel to within approximately 2.5 μm across 30 mm (83 μrad). We note that the tolerable PV error across the mirror active area is considerably smaller (it is determined by the illumination footprint instead of mirror size); however, the PV errors listed in Table 2 are most relevant to assembly and fabrication tolerance.

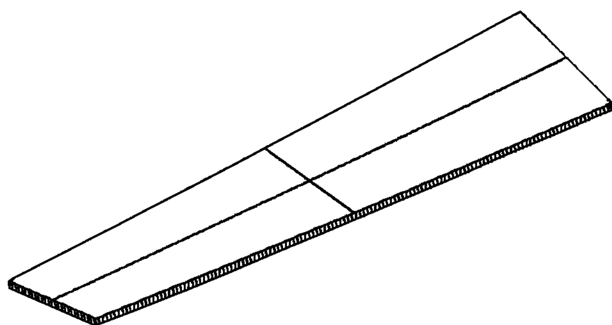

Fig. 5. Example of a twist error (magnitude exaggerated for visualization purposes).

Table 2. Twist Error Tolerance[a]

Twist Error	M5	M6
T	5.0×10^{-7} mm	8.8×10^{-7} mm
PV error	3.0 μm	5.3 μm

[a]Tabulation of both the twist coefficient and the PV deflection on one end of the mirror when the opposite end is assumed fixed.

Because on our K–B mirrors the twist actuation is performed from one end of the mirror only, there arises an interdependence between twist and roll as measured at the mirror center. This suggests the possible use of twist compensation to mitigate the effects of a roll error. To demonstrate the effectiveness of this compensation, we recalculate the roll tolerance using twist on the same mirror as compensation. This configuration is particularly relevant to our experimental situation in which the roll is fixed during assembly but twist control is available *in situ* for both mirrors. Table 3 shows that twist compensation increases the roll error tolerance considerably for M6, whereas it has virtually no effect for M5. The discrepancy in the behavior of the twist compensation between the two mirrors is because the vertically focusing M5 mirror must work in concert with the vertically focusing M2 mirror to provide the total 60× demagnification, whereas the horizontally focusing M6 works alone. A roll error on M5 causes interaction problems with both M2 and M6. This problem can be overcome when the entire K–B system is rolled such that the focusing axes of M5 and M2 are aligned. Under this condition the problem is effectively transformed to a roll error on M6 that we can readily correct using twist on M6. We note that the ability to roll the entire K–B system is present in the experimental system under consideration here. It is also important to note that this issue is irrelevant for stigmatic object plane K–B systems as used, for example, in the EUV mask defect inspection beamline at the Advanced Light Source.[10]

In addition to compensating for roll error, we can also use twist on one mirror to partially offset the effect of twist on the other mirror. Table 4 shows that the balanced twist tolerance is approximately

Table 4. Balanced Twist Error Tolerance

Twist Error	M5	M6
T	4.7×10^{-6} mm	8.3×10^{-6} mm
PV error	28 μm	50 μm

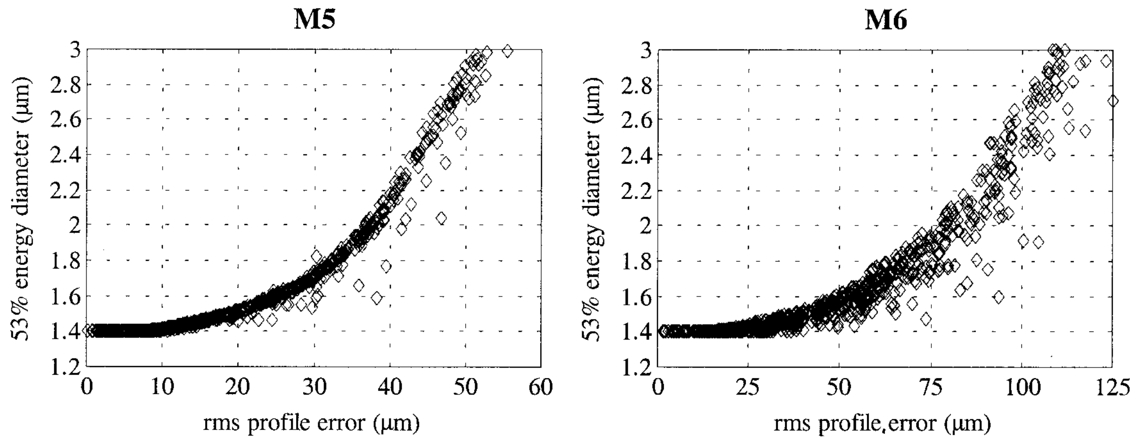

Fig. 6. CODE V calculation of the system response to random profile errors. We simulated 1000 realizations of the profile error. The plots show the 53% encircled energy disk diameter as a function of the rms width profile error for each mirror. In each case, the other mirror is assumed ideal.

ten times larger than the isolated twist tolerance. This result indicates that a significant benefit can be obtained even if twist correction is added to only one of the two mirrors.

Finally, we consider mirror bend errors. As stated above, the K–B system is composed of bendable mirrors that rely on *in situ* controllable bend moments applied to the ends of the mirror so they can attain their ideal shapes. This shaping relies strongly on the width profiling and thickness uniformity of the mirror. Based on bent-beam theory, the curvature of the bent mirror can be shown to be inversely proportional to the cross-section moment of inertia of the mirror cross section. The mirror cross-section moment of inertia, in turn, is directly proportional to the mirror width and proportional to the mirror thickness cubed.[14–16] In practice, mirror width profiling tends to be more difficult to achieve than mirror flatness; hence we numerically consider system tolerance for the profiling errors only. Moment of inertia errors for both profile and thickness have been addressed analytically in the literature.[14,16]

We performed a statistical investigation by adding a randomly generated error term to the ideal mirror profile and then determining the effect this profile error has on the point-spread function after least-squares optimization of the bend couples. Because of particulars of the CODE V implementation of the bendable K–B mirror, the error is added to the sag as a tenth-order polynomial term, and the corresponding profile error is calculated. We note that the elastic beam bending equations used in the model require the profile variations to be small and gentle compared with the nominal profile width; therefore the ability to add higher-frequency error terms would likely not provide meaningful results.

We create each individual realization of the error by generating ten normally distributed random numbers used as fractional error coefficients added to the ideal sag polynomial. Running the simulation to produce approximately 1000 realizations of the profile error, we generated the data plotted in Fig. 6. The plots show the 53% encircled energy disk diameter as a function of the rms width profile error for each mirror. In each case, the other mirror is assumed ideal, and the free parameters of the affected mirror (tilts and bends) were optimized. Table 5 lists the width profile error tolerance derived from the plots in Fig. 6. The tolerances in Table 5 are determined when we take all values of the 53% encircled energy disk diameter falling within ±5% of two times the error-free diameter of 1.4 μm and average the corresponding rms profile error values. The quoted uncertainties are based on the standard deviation of the corresponding rms profile error values.

We note that the tolerances described above assume isolated errors in an otherwise ideal system. In practice, when multiple errors are present the tolerance to each individual error would be reduced accordingly, with the exception of the error-balancing situations described above.

4. Error Signatures

To align a K–B system, such as the one described above, it is essential for the operator to recognize the error signatures for at least the parameters under operator control. In this section we use CODE V to

Table 5. Tolerance to rms Width Profile Error Assuming a Nominal Mirror Width of 30 mm[a]

Profile Error	M5	M6
rms	(49 ± 1.5) μm	(110 ± 7.0) μm
Fractional rms	(0.16 ± 0.005) %	(0.37 ± 0.023) %

[a]Reported values are derived from the plots in Fig. 6. The tolerances are determined when we take all values of the 53% encircled energy disk diameter falling within ±5% of two times the error-free diameter of 1.4 μm and average the corresponding rms profile error values. The quoted uncertainties are based on the standard deviation of the corresponding rms profile error values.

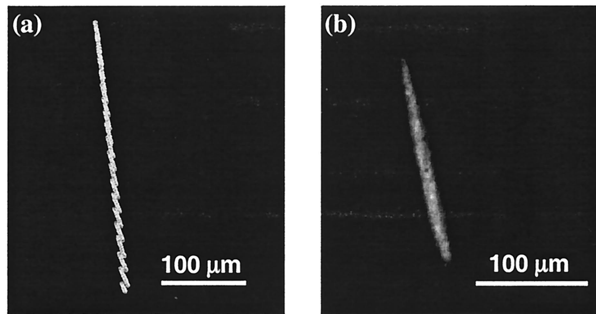

Fig. 7. (a) CODE V-calculated spot diagram of the image distribution when the M5 mirror has twist error and is intentionally defocused. The twist error is 26-μm PV relative to a fixed end at a length of 200 mm and across a width of 30 mm. This error magnitude is approximately equal to the error tolerance described in Table 4. The defocus is set to cause a PV sag error of 10 μm across the 200-mm mirror length. (b) Experimental results obtained under conditions set to nominally match the modeling parameters for (a). We recorded the image by placing a fluorescent YAG crystal in the image plane and reimaging the crystal to a CCD using a microscope objective.

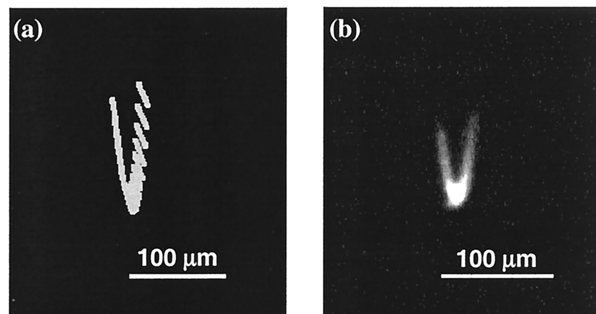

Fig. 8. (a) CODE V-calculated spot diagram for the same twist error as described in Fig. 7, but here one end of the mirror is overfocused causing the line to fold into a V shape. The twist causes light from the two extreme ends of the mirror to be directed to different points in the cross-focus direction (the x direction for the mirror under consideration). The separation that can be seen at the top of the V would be the effective image blur in the optimal focus position. (b) Experimental results obtained under conditions set to nominally match the modeling parameters for (a). The image was recorded as described in Fig. 7.

reveal these error signatures and show corresponding experimental results.

The obvious error, which we do not explicitly address here, is defocus. Defocus, in one or two dimensions, is clearly manifest as an expanded image. We consider, instead, twist and roll errors, which lead to less intuitive results.

As described above, twist error can be viewed as a roll error that changes as a function of position along the length of the mirror. One convenient way to visualize position-dependent errors on K–B mirrors is to slightly relax one mirror, which effectively collimates the beam in one direction while maintaining a relatively well-focused beam in the other direction. This achieves a mapping in the image plane where the image-plane position in the defocused direction essentially corresponds to y (length) along the relaxed mirror and x along the focused mirror. Slope errors on the mirrors will be manifest as distortions of the ideal one-dimensional defocused image (a straight line).

Figure 7(a) shows a CODE V-calculated spot diagram of an image distribution when the M5 mirror has twist error and is defocused and M6 is ideal. The twist error is set to 26-μm PV as described above. This twist error magnitude is close to the tolerance to compensated twist described in Table 4. The bend error (intentional defocus), equal on both ends, is set to cause a PV sag error of 10 μm across the 200-mm mirror length. The observed image is a tilted line, which comes from the position-dependent roll error causing the light to be deflected in the x direction of the mirror in question.

Figure 7(b) shows experimental results obtained under conditions set to nominally match the modeling parameters described above. We recorded the image by placing a fluorescent YAG crystal in the image plane and reimaging the crystal to a CCD using a microscope objective. Removing or balancing this twist error requires one to adjust the twist on one of the mirrors to remove the tilt from the observed line image. We note that the reference axis for the untilted line image can be determined experimentally by means of focusing the beam as well as possible in both directions and sweeping the mirror tilt adjustment. The image-plane axis defined by the moving spot should be used as the reference axis for the line image observed with the mirror defocused.

Figure 8(a) shows the CODE V-calculated intensity distribution for the same amount of twist, but in this case one end of the mirror is overfocused causing the line to fold over into a V shape. The twist causes light from the two extreme ends of the mirror to be directed to different points in the cross-focus direction (the x direction for the mirror under consideration). The beam separation that can be seen at the top of the V would be the effective image-point blur in the optimal focus position. Figure 8(b) shows the experimental results obtained under conditions set to nominally match the modeling parameters described for Fig. 7. Here, we can remove the twist by making the adjustments that collapse the V into a straight line. Because twist and roll errors are interdependent, as shown in Table 3, repeating the above exercise in the presence of roll error produces similar results.

5. Conclusion

A set of specifications required for the diffraction-limited performance of an operational EUV K–B system has been presented. The specifications are based on CODE V modeling tools developed expressly for grazing-incidence optical systems. In addition, error signatures as observed in the K–B focal plane have been presented, revealing possible *in situ* alignment strategies. The analysis showed that, given the tight fabrication and assembly tolerances on pa-

rameters such as tilt, roll, and twist, *in situ* alignment controls for some or all of these parameters is highly desirable. It was also shown that significant alignment flexibility can be gained when we simply add twist control to one of the two mirrors. Although the motivation and specific example presented here are based on EUV applications, the methods and results are broadly applicable to K–B systems operating in any wavelength range.

The authors are greatly indebted to Paul Denham, Gideon Jones, and Rene Delano for expert fabrication and assembly of the K–B focusing system, to David Richardson for the development of the software control system, and to the entire Center for X-Ray Optics staff for enabling this research. This research was supported by the Extreme Ultraviolet Limited Liability Company and the U.S. Department of Energy Office of Basic Energy Science.

References

1. R. Stulen and D. Sweeney, "Extreme ultraviolet lithography," IEEE J. Quantum Electron. **35,** 694–699 (1999).
2. J. H. Underwood and T. W. Barbee, Jr., "Layered synthetic microstructures as Bragg diffractors for X rays and extreme ultraviolet: theory and predicted performance," Appl. Opt. **20,** 3027–3034 (1981).
3. D. Attwood, G. Sommargren, R. Beguiristain, K. Nguyen, J. Bokor, N. Ceglio, K. Jackson, M. Koike, and J. Underwood, "Undulator radiation for at-wavelength interferometry of optics for extreme-ultraviolet lithography," Appl. Opt. **32,** 7022–7031 (1993).
4. J. E. Bjorkholm, A. A. MacDowell, O. R. Wood II, Z. Tan, B. LaFontaine, and D. M. Tennant, "Phase-measuring interferometry using extreme ultraviolet radiation," J. Vac. Sci. Technol. B **13,** 2919–2922 (1995).
5. A. K. Ray-Chaudhuri, W. Ng, F. Cerrina, Z. Tan, J. Bjorkholm, D. Tennant, and S. J. Spector, "Alignment of a multilayer-coated imaging system using extreme ultraviolet Foucault and Ronchi interferometric testing," J. Vac. Sci. Technol. B **13,** 3089–3093 (1995).
6. H. Medecki, E. Tejnil, K. A. Goldberg, and J. Bokor, "Phase-shifting point diffraction interferometer," Opt. Lett. **21,** 1526–1528 (1996).
7. K. A. Goldberg, E. Tejnil, S. H. Lee, H. Medecki, D. T. Attwood, K. H. Jackson, and J. Bokor, "Characterization of an EUV Schwarzschild objective using phase-shifting point diffraction interferometry," in *Emerging Lithographic Technologies*, D. E. Seeger, ed., Proc. SPIE **3048,** 264–270 (1997).
8. P. Naulleau, K. Goldberg, E. Gullikson, and J. Bokor, "At-wavelength, system-level flare characterization of extreme-ultraviolet optical systems," Appl. Opt. **39,** 2941–2947 (2000).
9. E. M. Gullikson, "Scattering from normal incidence EUV optics," in *Emerging Lithographic Technologies II*, Y. Vladimirski, ed., Proc. SPIE **3331,** 72–80 (1998).
10. S. Jeong, L. Johnson, S. Rekawa, C. Walton, S. Prisbrey, E. Tenjil, J. Underwood, and J. Bokor, "Actinic detection of sub-100 nm defects on extreme ultraviolet mask blanks," J. Vac. Sci. Technol. B **17,** 3009–3013 (1999).
11. J. Underwood and E. Gullikson, "Beamline for measurement and characterization of multilayer optics for EUV lithography," in *Emerging Lithographic Technologies II*, Y. Vladimirski, ed., Proc. SPIE **3331,** 52–61 (1998).
12. P. Kirkpatrick and A. Baez, "Formation of optical images by x-rays," J. Opt. Soc. Am. **38,** 766–774 (1948).
13. W. Ehrenberg, "X-ray optics: the production of converging beams by total reflection," J. Opt. Soc. Am. **39,** 741–745 (1949).
14. J. Underwood, "Generation of a parallel x-ray beam and its use for testing collimators," Space Sci. Instrum. **3,** 259–270 (1977).
15. M. R. Howells and D. Lunt, "Design considerations for adjustable-curvature, high-power, x-ray mirrors based on elastic bending," Opt. Eng. **32,** 1981–1989 (1993).
16. M. R. Howells, D. Cambie, R. Duarte, S. Irick, A. A. MacDowell, H. A. Padmore, T. R. Renner, S. Rah, and R. Sandler, "Theory and practice of elliptically bent x-ray mirrors," Opt. Eng. **39,** 2748–2761 (2000).
17. CODE V is a registered trademark of Optical Research Associates, 3280 E. Foothill Blvd., Pasadena, Calif. 91107.
18. D. Attwood, P. Naulleau, K. Goldberg, E. Tejnil, C. Chang, R. Beguiristain, P. Batson, J. Bokor, E. Gullikson, H. Medecki, and J. Underwood, "Tunable coherent radiation in the soft X-ray and extreme ultraviolet spectral regions," IEEE J. Quantum Electron. **35,** 709–720 (1999).
19. B. Lai and F. Cerrina, "SHADOW: a synchrotron radiation ray tracing program," Nucl. Instrum. Methods Phys. Res. A **246,** 337–341 (1986).
20. *CODE V Version 8.30 Reference Manual* (Optical Research Associates, Pasadena, Calif., 1998), Chaps. 2A, 11C, 11D.